Application of Zernike polynomials towards accelerated adaptive focusing of transcranial high intensity focused ultrasound

Elena A. Kaye[a)]
Department of Radiology, Stanford University, Stanford, California 94305
and Department of Electrical Engineering, Stanford University, Stanford, California 94305

Yoni Hertzberg
School of Physics and Astronomy, Tel-Aviv University, Tel-Aviv, 61999 Israel

Michael Marx
Department of Radiology, Stanford University, Stanford, California 94305
and Department of Electrical Engineering, Stanford University, Stanford, California 94305

Beat Werner
MR-Center, University Children's Hospital, Zurich, 8032 Switzerland

Gil Navon
School of Chemistry, Tel-Aviv University, Tel-Aviv, 61999 Israel

Marc Levoy
Department of Computer Science, Stanford University, Stanford, California 94305

Kim Butts Pauly
Department of Radiology, Stanford University, Stanford, California 94305

(Received 10 February 2012; revised 7 August 2012; accepted for publication 26 August 2012; published 27 September 2012)

Purpose: To study the phase aberrations produced by human skulls during transcranial magnetic resonance imaging guided focused ultrasound surgery (MRgFUS), to demonstrate the potential of Zernike polynomials (ZPs) to accelerate the adaptive focusing process, and to investigate the benefits of using phase corrections obtained in previous studies to provide the initial guess for correction of a new data set.

Methods: The five phase aberration data sets, analyzed here, were calculated based on preoperative computerized tomography (CT) images of the head obtained during previous transcranial MRgFUS treatments performed using a clinical prototype hemispherical transducer. The noniterative adaptive focusing algorithm [Larrat *et al.*, "MR-guided adaptive focusing of ultrasound," IEEE Trans. Ultrason. Ferroelectr. Freq. Control **57**(8), 1734–1747 (2010)] was modified by replacing Hadamard encoding with Zernike encoding. The algorithm was tested in simulations to correct the patients' phase aberrations. MR acoustic radiation force imaging (MR-ARFI) was used to visualize the effect of the phase aberration correction on the focusing of a hemispherical transducer. In addition, two methods for constructing initial phase correction estimate based on previous patient's data were investigated. The benefits of the initial estimates in the Zernike-based algorithm were analyzed by measuring their effect on the ultrasound intensity at the focus and on the number of ZP modes necessary to achieve 90% of the intensity of the nonaberrated case.

Results: Covariance of the pairs of the phase aberrations data sets showed high correlation between aberration data of several patients and suggested that subgroups can be based on level of correlation. Simulation of the Zernike-based algorithm demonstrated the overall greater correction effectiveness of the low modes of ZPs. The focal intensity achieves 90% of nonaberrated intensity using fewer than 170 modes of ZPs. The initial estimates based on using the average of the phase aberration data from the individual subgroups of subjects was shown to increase the intensity at the focal spot for the five subjects.

Conclusions: The application of ZPs to phase aberration correction was shown to be beneficial for adaptive focusing of transcranial ultrasound. The skull-based phase aberrations were found to be well approximated by the number of ZP modes representing only a fraction of the number of elements in the hemispherical transducer. Implementing the initial phase aberration estimate together with Zernike-based algorithm can be used to improve the robustness and can potentially greatly increase the viability of MR-ARFI-based focusing for a clinical transcranial MRgFUS therapy. [http://dx.doi.org/10.1118/1.4752085]

Key words: transcranial, MRgFUS, MR-ARFI, Zernike polynomials, adaptive focusing

I. INTRODUCTION

Magnetic resonance imaging guided focused ultrasound surgery (MRgFUS) is an attractive technique for the treatment of various pathologies, including uterine fibroids,[1] breast tumors,[2–4] liver tumors,[5] and a range of brain pathologies[6,7] due to its noninvasiveness and the absence of ionizing radiation. In recent clinical trials, MRgFUS was used to treat neuropathic pain,[6] brain tumors,[7] and essential tremors. Historically, delivering ultrasound energy to targets inside the brain has been challenging because of the adverse effects that the skull bone has on the propagation of the ultrasound field. The inhomogeneity of the acoustic properties of the calvarium causes amplitude and phase aberrations of the ultrasound beam, which affect the position, shape, and intensity of the acoustic focus. To overcome the detrimental effects of the skull on transcranial ultrasound focusing, modern phased-array transducers[8–10] are designed with a large number of elements, which can be individually phased to compensate for aberrations caused by the skull.

Two general approaches to determining optimal transducer elements' phase settings for correcting aberration have been explored to date. One relies on estimating local aberrations using an acoustic model of the patient's skull, obtained from MR (Refs. 11 and 12 or computerized tomography (CT) (Refs. 13–16) images of the head prior to MRgFUS treatment and calculating individual transducer element's phases based on simulated wave propagation. Accurate aberration estimation was demonstrated *ex vivo* using a 3D finite differences numerical simulation.[13,16] The other approach uses adaptive focusing algorithms[17–19] that manipulate the relative phase delays and sometimes the amplitudes of the individual transducer element's emissions until the pressure at the desired location is maximized. The pressure, or rather the acoustic intensity, at the acoustic focus is measured indirectly and noninvasively using a dedicated MRI technique known as MR acoustic radiation force imaging (MR-ARFI).[20–22] This imaging technique is sensitive to the displacement of tissue caused by acoustic radiation force, which is proportional to the local acoustic intensity of ultrasound and to the square of the local acoustic pressure. This technique uses motion-sensitive encoding gradients to encode the displacement of tissue as phase shifts in the MR image.

The CT-based aberration correction approach has already been used in clinical studies of transcranial MRgFUS.[6,7] However, acquisition of the high resolution CT images exposes the patient to ionizing radiation without diagnostic indication. Moreover, the CT-based modeling approach can require up to several hours of computation time[16] and relies on the accuracy of the acoustic model of the skull, transducer alignment, and intraoperative registration of CT and MR images. Since the acoustic model does not take into account potential dephasing caused by the presence of gas bubbles or electronic and mechanical misalignment, CT-based phase correction method was shown to result in suboptimal correction as compared to adaptive focusing approaches in *ex vivo* studies.[17,18] MR-ARFI-based adaptive focusing is of interest as it does not require a presurgical CT scan and it can provide superior correction.[18,19] However, current approaches require the acquisition of as many as 4 × N MR-ARFI images,[17,19] where N is number of transducer elements, which for current clinically used large phased-array transducers is either 512 or 1024 elements. Acquisition of such large numbers of images is very time consuming and adds significantly to total table time for the patient. Therefore, there is a critical need to reduce the total scan time for the adaptive focusing approach to be suitable for clinical applications.

The purposes of this work were to study the phase aberrations produced by human skulls during a transcranial MRgFUS phase I clinical study and to demonstrate the potential of Zernike polynomials (ZPs) (Ref. 23) to accelerate the adaptive focusing process. ZPs are commonly used in microscopy,[24] astronomy,[25,26] and ophthalmology[27] to describe wave front aberrations. In the first part of this study, the skull thickness and the corresponding phase aberration data from five patients are examined. Similarities and differences between different subjects are assessed qualitatively and quantitatively by looking at the correlations between different data sets. In the second part, a noniterative adaptive focusing approach based on ZPs is introduced and tested with five patient data sets using simulation of the clinical hemispherical phased-array transducer. The effect of the Zernike-based phase aberration correction on acoustic intensity at the focus is then visualized experimentally *ex vivo* using MR-ARFI. Finally, the potential benefit of using phase corrections obtained in previous studies to provide the initial guess for correction of a new data set is tested.

II. BACKGROUND AND THEORY

The total pressure at the acoustic focus of a phased-array transducer is the superposition of the spherical waves emitted by each transducer element. In the ideal case, when there are no aberrations, it can be written as

$$p_{\text{ideal}} = \sum_{i=1}^{N} e_i, \tag{1}$$

where e_i is the emission signal of a single element consisting of amplitude and phase. Skull aberrations perturb this relationship, so the total pressure becomes

$$p = \sum_{i=1}^{N} g_i \cdot e_i, \tag{2}$$

where g_i is a complex coefficient that relates the emitted waves of the transducer element i with its effective contribution to the resulting field in the acoustic focus,[17] and thus represents the aberration experienced by this wave. The magnitude of g_i corresponds to acoustic attenuation, while the angle of g_i corresponds to phase aberration. Correcting for these coefficients in the emissions e_i will compensate for the aberrations. Phase aberrations are corrected by shifting the phases of each element's emission signals, e_i, by the opposite of the phase of g_i.

Adaptive focusing with MR-ARFI has been demonstrated using iterative[18] and noniterative[17] approaches *ex vivo*. In the

iterative approach,[18] the phase shifts of small groups of transducer elements are adjusted sequentially using an iterative optimization algorithm until displacement, and thus pressure, is maximal at the focal spot. In the noniterative approach,[17] the optimal transducer phases are derived analytically based on a set of reference measurements. In the original approach presented by Larrat *et al.*,[17] a Hadamard matrix **H** is used to encode groups of transducer elements into N virtual transducers. The resulting pressure at the focus, p, is given by

$$p = \sum_{i=1}^{N} g_i \cdot h_i, \tag{3}$$

where h_i are the elements of the column vectors $\mathbf{h}_i$ of the Hadamard matrix encoding the virtual transducers. For each encoded emission, the pressure, p, is determined noninvasively using MR-ARFI.[17] The complex aberration coefficients, g_i, are then found by solving Eq. (3). Using the notation introduced by Larrat *et al.*,[17] the equation can be presented in matrix form

$$\mathbf{p}^H = \mathbf{g} \cdot \mathbf{H}, \tag{4}$$

where $\mathbf{p}^H$ is a vector of focal pressures measured during the encoded emissions $\mathbf{h}_i$. After visual inspection of the skull phase aberration patterns, presented in this study, we propose to replace the Hadamard encoding with an encoding basis potentially more representative of skull phase aberrations consisting of Zernike polynomials.

ZPs are an infinite set of two-dimensional, rotationally invariant[28] polynomials that form a complete, orthogonal basis over the unit disk. On a continuous unit circle, ZPs are described by the equations

$$Z_n^m(\rho,\theta) = \begin{cases} \sqrt{2(n+1)}ZR_n^m(\rho)\cos(m\theta) & \text{for } m > 0 \\ \sqrt{2(n+1)}ZR_n^m(\rho)\sin(|m|\theta) & \text{for } m < 0, \\ \sqrt{(n+1)}ZR_n^m(\rho) & \text{for } m = 0 \end{cases} \tag{5}$$

where n is the radial polynomial order and m is the azimuthal frequency. The radial Zernike polynomial, ZR_n^m, is defined as

$$ZR_n^m(\rho) = \sum_{s=0}^{(n-|m|)/2} \frac{(-1)^s (n-s)!}{s!\left(\frac{n+|m|}{2}-s\right)!\left(\frac{n-|m|}{2}-s\right)!}\rho^{n-2s}. \tag{6}$$

The first five modes of ZPs are shown in Fig. 1. To simplify notation in this work, the Malacara indexing system[29] is used when referring to specific polynomials. Polynomials are arranged into a sequence of increasing radial orders and frequency and are given a mode number reflecting their order in the sequence. For example, Z_0^0, Z_1^{-1}, Z_1^1, Z_2^{-2}, Z_2^0, Z_2^2 become Z_1, Z_2, Z_3, Z_4, Z_5, Z_6. The dotted arrows in Fig. 1 show the order in which ZPs are sorted into a sequence of Z_k polynomials.

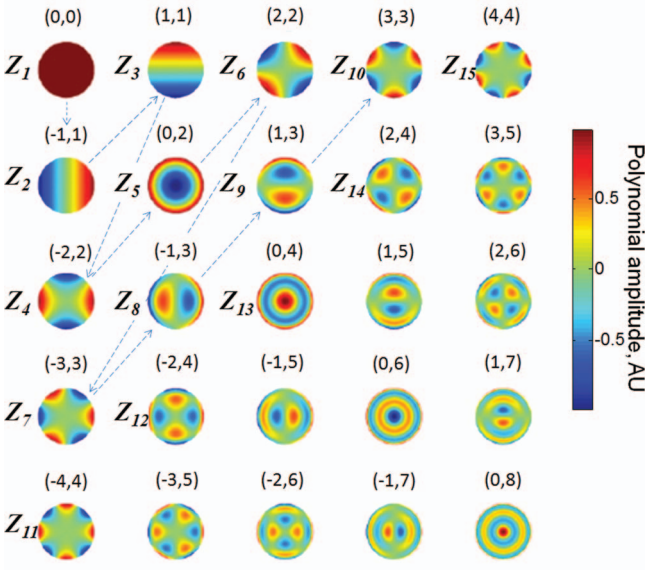

FIG. 1. Zernike polynomials computed for the first five radial orders, m, and azimuthal frequencies, n. Order and frequency indices m and n are shown in parenthesis as (m,n). Dotted lines show the sequential order of the polynomial modes used in this work, which are labeled as Z_1, Z_2, and so on.

III. MATERIALS AND METHODS

III.A. Analysis of acoustic aberrations in the human skull

The phase correction data obtained during five transcranial MRgFUS treatments, previously described by Martin *et al.*,[6] was reused in this work. During these treatments, patients underwent a selective central lateral thalatomy performed using a clinical prototype FUS system (ExAblate 4000, InSightec, Tirat Carmel, Israel) integrated into a 3 T MRI scanner (GE, Milwaukee).[6] The FUS system consisted of a hemispheric 1024-element phased-array transducer, shown schematically in Fig. 2(a), operating at a central frequency of 650 kHz. The phase aberrations experienced by acoustic waves emitted from each transducer element were evaluated using a ray acoustic model made of various layers of different acoustic characteristics. The acoustic properties of the layers were obtained by analyzing the preoperative CT images of patient's head.[14] The mean and the standard deviation of phase aberration values across all elements were calculated for each subject. Fully anonymized CT data sets of the patients were used to obtain thickness maps of the skulls, calculated as the distance between the inner and outer surfaces of the skull. The inner and outer surfaces were segmented using a threshold of 476 Hounsfield units. The most superior slices of CT data set, approximately corresponding to the part of the skull expected to be inside the hemispherical trasnducer, were segmented. After segmentation, the coordinates of the inner and outer boundaries of the skull were processed using GeoMagic (Geomagic Inc.) 3D software. The inner and outer surfaces were constructed from the boundary coordinates, and the distance between the two surfaces was calculated based on the nearest point approach.

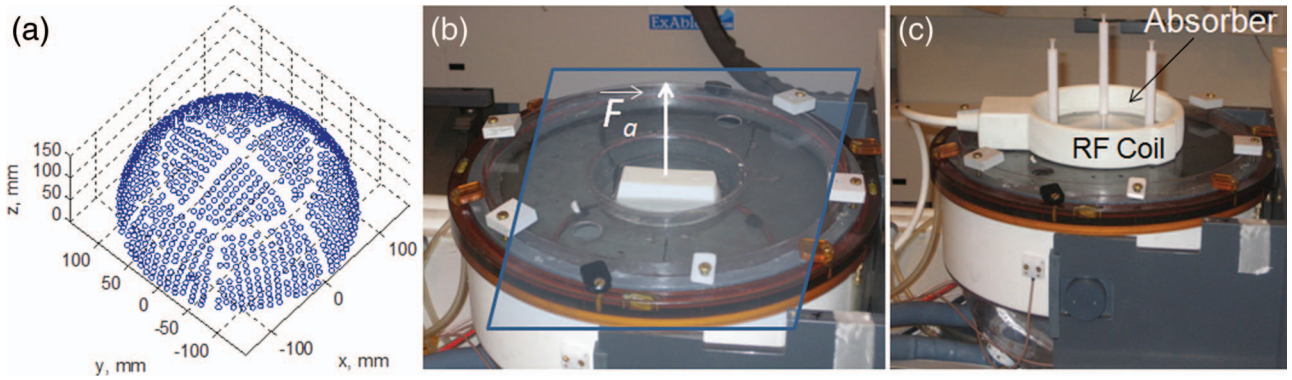

FIG. 2. (a) Positions of the elements of the hemispherical phased-array transducer (ExAblate 4000, InSightec, Tirat Carmel, Israel). Experimental setup: (b) Hemispherical transducer is filled with degassed water and closed with a transparent lid. The tissue mimicking phantom is placed in the natural focus of the transducer, i.e., the center of the hemisphere. The imaging plane is perpendicular to the acoustic radiation force vector F_a, shown with white arrow. Displacement encoding is performed along the direction of acoustic radiation force, (c) An acoustic absorber is placed over the phantom and the RF coil is positioned around the absorber.

Correlation coefficients were calculated between the aberration values for every pair of data sets, using a MATLAB function computing correlation coefficients based on covariance (corrcoef.m).

III.B. Simulation of noniterative adaptive focusing algorithm based on Zernike encoding

In this part of the work, discrete Zernike polynomials were calculated using the Matlab Zernike function (zernfun.m) (Ref. 30) which implements the analytical expressions in Eqs. (5) and (6). The polynomials were sampled at the (x, y) locations of each element of the hemispherical transducer. These locations are plotted in Fig. 2(a). Since orthogonality of continuous ZPs is perturbed by discrete sampling,[31,32] the Gram-Schmidt process was used to orthonormalize the discrete polynomials. Their mutual orthogonality was tested by computing the Gram matrix before and after orthonormalization.

To apply ZPs in the adaptive focusing algorithm, which is explained in detail using Hadamard encoding by Larrat *et al.*,[17] a full rank N by N Zernike matrix, $\mathbf{Z}$, was constructed using the orthonormalized discrete ZPs,

$$\mathbf{Z} = \left[Z_1^T Z_2^T \cdots Z_i^T \cdots Z_N^T \right]. \tag{7}$$

Here Z_i^T is an orthonormalized discrete ZP of mode i, written as a column vector with superscript T indicating vector transposition. Using notation introduced in Ref. 17 and Zernike encoding, the relationship described by Eq. (4) can be rewritten as

$$\mathbf{p}^Z = \mathbf{g} \cdot \mathbf{Z}. \tag{8}$$

In order to estimate $\mathbf{g}$, the phase delays of each Z_i^T emission can be optimized relative to a reference emission Z_1^T. The values of $\mathbf{p}^Z$ are inferred by measuring the intensity of the field produced by the superposition of each Z_i^T with the reference emission. The pressure, p_1^Z, produced by the first virtual transducer emission, Z_1^T, is referred to in this work as reference pressure with an amplitude of 1 and a phase of 0. Using a method described by Larrat *et al.*,[17] four intensity measurements I_i^a, I_i^b, I_i^c, and I_i^d are necessary for each Z_i^T emission combination in order to estimate phase and amplitude of $\mathbf{p}^Z$. The four transmit superpositions $s_i^a, s_i^b, s_i^c, s_i^d$ that are used to obtain the four desired intensity measurements are

$$s_i^a = \left(Z_1^T + Z_i^T\right), \quad s_i^b = \left(Z_1^T - Z_i^T\right),$$
$$s_i^c = \sqrt{2}\left(Z_1^T + jZ_i^T\right), \quad s_i^d = \sqrt{2}\left(Z_1^T - jZ_i^T\right). \tag{9}$$

In Hadamard encoding, half of the elements will transmit at full power while half of the elements will be turned off for each of the four superpositions. In Zernike encoding, transmission amplitude for the elements, s_i, varies continuously between zero and one, not necessarily reaching one for every Zernike mode. It would be inefficient signal-to-noise ratio (SNR)-wise to use maximum emission powers less than the maximum transducer element power. Therefore, to take advantage of the full dynamic range of the transducer, scaling coefficients c_i^a, c_i^b, c_i^c, and c_i^d are applied to s_i^a, s_i^b,s_i^c, and s_i^d to maximize the maximum amplitude of each transmission. Once the measurements of I_i^a, I_i^b, I_i^c, and I_i^d are collected, they are scaled by the inverse of $(c_i)^2$ in order to get the measurement we would have obtained if no c_i scaling was used. The use of scaling coefficients relies on a linear relationship between applied power and the displacement phase measured with MR-ARFI.[33]

After making the four intensity measurements, $\mathbf{p}^Z$ can be calculated using

$$\mathrm{Re}\left(p_i^Z\right) = \frac{1}{2}\rho c\left(\frac{I_i^a}{c_i^{a^2}} - \frac{I_i^b}{c_i^{b^2}}\right) \text{ and}$$
$$\mathrm{Im}\left(p_i^Z\right) = \frac{1}{4}\rho c\left(\frac{I_i^d}{c_i^{d^2}} - \frac{I_i^c}{c_i^{c^2}}\right). \tag{10}$$

Equation (10) takes into account the density, ρ, and the speed of sound, c, of the tissue of interest. The aberrations vector $\mathbf{g}$ can be calculated as

$$\mathbf{g} = \mathbf{p}^Z \cdot \mathbf{Z}^{-1}, \tag{11}$$

where the phase and amplitude of **g** represent the phase and relative amplitude of the aberrations for each of the N elements of the array of emitting transducers.

The Zernike-encoding-based algorithm for estimation of aberrations was tested using a simulated ExAblate 4000 hemispherical transducer (Fig. 2), modeled in MATLAB using the Rayleigh-Sommerfield method.[34] The transducer was simulated in a monochromatic regime (710 kHz) and focused on the natural focus of the hemisphere. The choice of the central frequency 60 kHz higher than the frequency of the transducer used in the clinical study from which the phase aberrations were obtained was based on the frequency of the hemispherical transducer available during this study (see Sec. III.C). Though calculated for a transducer of 60 kHz lower frequency, the phase aberrations were considered representative for 710 kHz case. The speed of sound of the medium was simulated as 1500 m/s. The pressure field at the focus, calculated on a 5 by 5 mm grid with a spatial step of 0.1 mm, was converted to intensity by taking the square of pressure. The complex values of p_i^Z at the focus were calculated for each Zernike-encoded emission, Z_i^T. The influence of the number of ZP modes used for aberration correction was studied by implementing the algorithm with the number of ZP modes, N_{zp}, increasing from 1 to N, where N is 960, the number of active elements in the 1024-element transducer. For each set of Zernike polynomials, Eq. (11) was solved using an N by N inverse of a Zernike matrix and $\mathbf{p}^Z$ vector, with p_i^Z values set to zero for i greater than N_{zp}, the number of Zernike-encoded emissions used. Then, corrections were calculated using ZPs up to mode N_{zp}. Phase correction was applied to compensate for the patient's phase aberration. Relative intensity was calculated as the ratio of intensity after correction to intensity without aberrations.

III.C. Experimental validation of the effect of phase correction computed using Zernike encoding

The effect of phase aberration correction values calculated using the Zernike-based adaptive focusing algorithm on focal point intensity was studied experimentally in a gel phantom using MR-ARFI to measure acoustic intensity in the focus. Phase aberration values obtained in the treatment of subject 1 were applied to the hemispherical transducer and then compensated for using the phase correction values calculated in the simulations described in Sec. III.B. Displacement measurements were performed for phase corrections using the following increasing number of ZP modes: 4, 10, 30, 50, 70, 90, 110, 130, 200, 500, 700, and 960, where 960 is N, the number of active elements in the transducer.

Measurements were performed using the hemispherical transducer (ExAblate 4000, InSightec, Tirat Carmel, Israel) placed vertically into a 1.5 T MRI scanner (GE, Milwaukee) and filled with degassed water. This transducer operated at 710 kHz. A tissue-mimicking phantom based on 5% fat milk (Malabi Dairy Dessert of Gad Dairies, Bat-Yam, Israel) was positioned in the plane of the natural focus using a holder as shown in Fig. 2(b). An acoustic absorber was placed on top of the phantom [Fig. 2(c)] to avoid interfering reflections.

Tissue displacement phase was imaged using a 2D Fourier transform spin-echo MR-ARFI pulse sequence with repeated bipolar displacement encoding gradients.[35] Displacement encoding gradients were applied along the dominant direction of the ultrasound induced radiation force, as shown with an arrow in Fig. 2(b). The duration of each encoding lobe was 6.1 ms, the duration of the ultrasound pulse was 19 ms. Imaging was performed using a solenoid breast RF coil in a transverse plane relative to the ultrasound. The following imaging parameters were used: TE = 41 ms, TR = 500 ms, FOV = 30 × 20 cm, matrix size = 256 × 82, BW = 15.63 kHz, and slice thickness = 6 mm. Total acquisition time was 50 s for each phase correction. The displacement phase at the focal spot was calculated as displacement phase signal averaged over 3 × 2 pixels. The displacement phase signal-to-noise ratio was computed as the ratio of the average displacement phase at the focal spot to the displacement phase noise. The noise was calculated as standard deviation of displacement phase in a 50 by 30 pixels region of interest outside of the focal spot.

III.D. Initial guess for noniterative adaptive focusing algorithm based on existing phase aberration data

In this section, we tested whether phase aberration data obtained from previous subjects can be used to construct an initial phase aberration estimate for a new subject. Two methods were investigated. First, using aberration data from five subjects, the initial phase aberration estimate for each subject was calculated as the average of the other four subjects' aberrations. Second, the data sets were separated into groups, based on the magnitude of the correlation coefficients between each pair of the subjects. In each group, the initial estimate was the average of the phase corrections of the remaining subjects in the group. Using these methods of constructing the initial guess phase aberration, the adaptive focusing Zernike-based algorithm was implemented and the relative intensity values after correction were calculated as described in Sec. III.B. The number of ZP modes necessary to achieve relative intensity 90% of the nonaberrated case was calculated for each subject and each initial estimate method.

IV. RESULTS

IV.A. Analysis of acoustic aberrations in the human skull

Skull thickness maps calculated by segmentation of the five patients' head CT images are shown in Fig. 3(a). These data are presented here to relate the phase aberration data from the clinical studies [Fig. 3(b)] to individual subjects' cranium morphology. Qualitative comparison of the shapes and variations of thickness across the five skulls shows a range of differences in the shape, size, and bone thickness. Despite these differences, some thickness variation patterns can be recognized in all of the skulls. For example, there is thickening in the posterior medial section of the skull in all five subjects. Some skull thickness variation patterns observed in

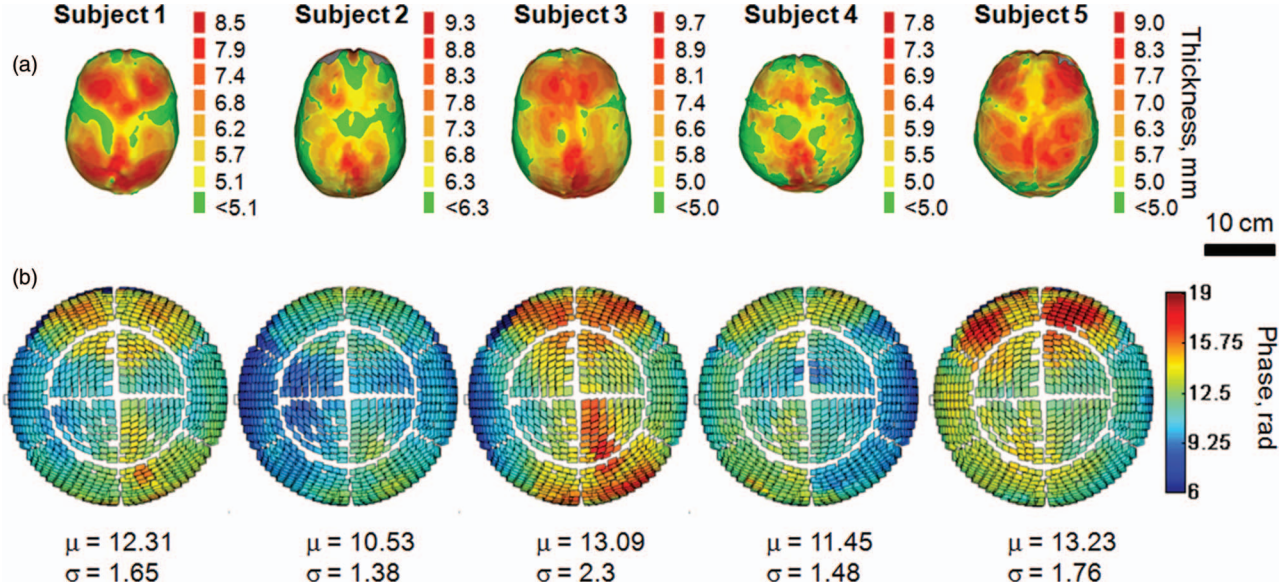

FIG. 3. Skull data of five patients: (a) skull thickness map displayed on the surface of the skull, calculated by segmenting head CT images of the patients (color scales are different across five subjects); (b) unwrapped phase aberration data calculated for each element of the hemispherical transducer during the MRgFUS treatments based on ray acoustic model made of various layers having different acoustic characteristics, which were obtained by analyzing the preoperative CT images of the patients. Small rectangular tiles schematically represent the elements of the transducer. The mean and the standard deviation of phase aberration data set are given for each patient.

Fig. 3(a) can also be observed in the phase aberration values seen by each transducer element, shown in Fig. 3(b). The average phase aberration, computed for each subject using unwrapped phase aberration data, varied between 10.53 rad and 13.23 rad with standard deviations varying between 1.38 rad and 2.3 rad.

The correlation coefficients across pairs of subjects are displayed graphically in Fig. 4. The correlation results suggest that these five data sets can be divided into two groups based on the level of correlation between the data. Correlation coefficients for subjects 1, 2, and 3 are greater than 0.8 and can be grouped together. Subjects 4 and 5 have a correlation coefficient of 0.65, and can be grouped together as well. The correlation between any two subjects across the two groups is less than 0.4.

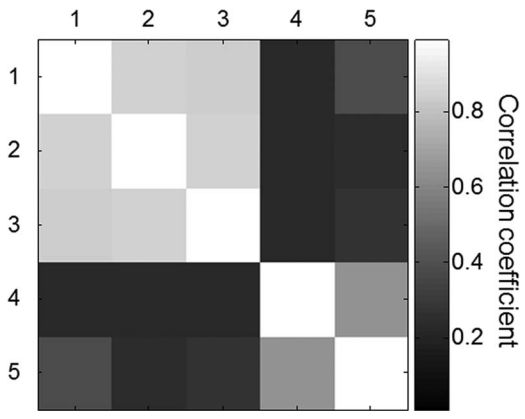

FIG. 4. Graphic representation of the correlation coefficients between phase aberration data from the five subjects, showing that subjects 1, 2, and 3 have phase aberration patterns more similar to each other than subjects 4 and 5.

IV.B. Simulation of noniterative adaptive focusing algorithm based on Zernike encoding

Example Zernike polynomials Z_2 and Z_{12} calculated for (x,y) coordinates of the hemispherical transducer are shown in Fig. 5(a), normalized such that the norm of each polynomial was equal to 1. The Gram matrix, expected to be an identity matrix for a set of orthonormal vectors, exhibited several nonzero entries [Fig. 5(b)] below and above the main diagonal, indicating compromised orthogonality of the set. This was corrected using the Gram-Schmidt orthogonalization

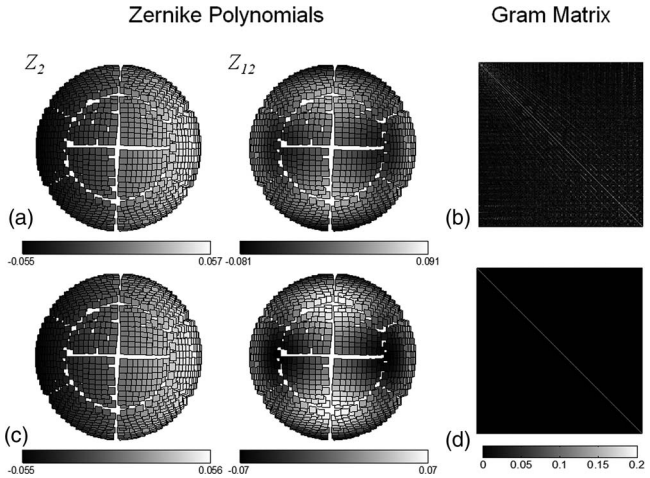

FIG. 5. (a) Two examples of normalized Zernike polynomials sampled at (x, y) coordinates of the hemispherical transducer displayed using different scales. (b) Gram matrix calculated for a set of normalized Zernike polynomials indicates compromised orthogonality. (c) Zernike polynomials and (d) Gram matrix after orthonormalization using Gram-Schmidt process.

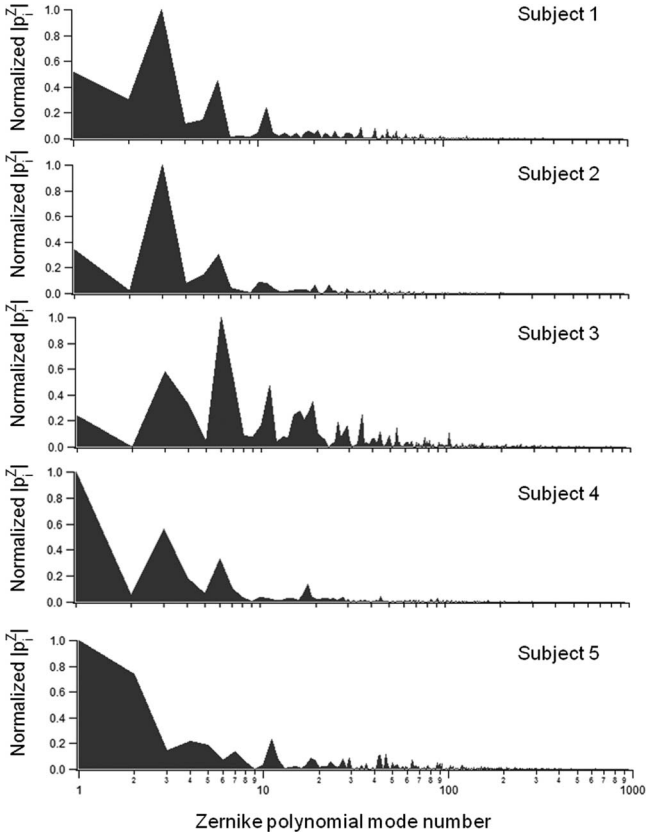

FIG. 6. Normalized values of $|p_i^Z|^2$ calculated for each Zernike-encoded emission up to the 960th mode for the phase aberration examples of subjects 1–5.

process, and the new Z_2 and Z_{12} polynomials and new Gram matrix are shown in Figs. 5(c) and 5(d).

The squared absolute values of p_i^Z, simulated at the focus for the five aberration cases, normalized by the highest value for each data set, are shown in Fig. 6. These results indicate the relative contribution of each mode of ZPs to the overall aberration correction. These values also correspond to the squared absolute values of expansion coefficients if phase aberration data were expressed using Zernike polynomials as the basis. It can be seen that for all of the five examples of aberration, the intensities resulting from the emissions encoded with the lower modes of ZPs have the highest values, thus pointing at the greater correction effectiveness of the low modes of ZPs. The greater effect of low-mode Zernike correction on the intensity at the focal spot can be observed in Fig. 7. The relative intensity for each of the five examples achieves 90% of nonaberrated intensity using fewer than 170 modes of ZPs.

IV.C. Experimental validation of the effect of phase correction computed using Zernike encoding

Figure 8(a) shows the displacement phase images obtained after compensating for the phase aberration of subject 1 with phase correction values computed using an increasing number of ZPs. The average displacement phase at the focal spot, normalized such that the maximum displacement of the nonaberrated case is 1, is shown in Fig. 8(b). The displacement phase SNR was 21 without phase aberration and 15.5 with phase aberration numerically applied. Similar to the intensity calculated using simulations, the behavior of the displacement phase at the focal spot indicates that the effect of the lower modes of ZPs on aberration correction is much greater than that of the higher modes. Ninety percent of the nonaberrated displacement phase is achieved while correcting the aberrations of subject 1 with aberration corrections estimated using fewer than 200 modes of ZP.

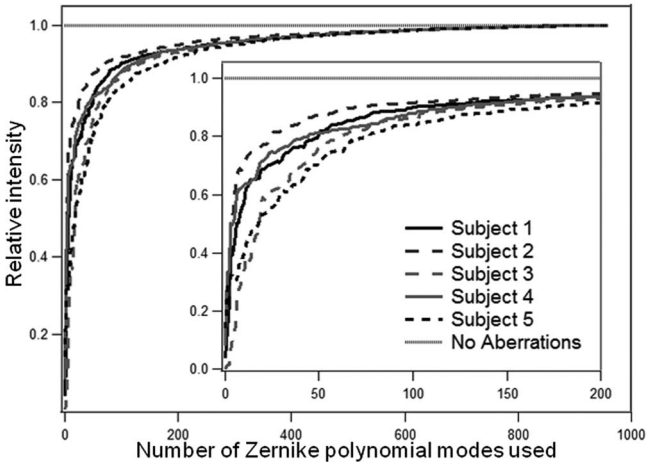

FIG. 7. Relative acoustic intensity at the focus plotted against the number of ZP modes used for aberration correction for ZP modes up to 960th mode. Insert plot shows the intensity values up to 200th ZP mode.

IV.D. Initial guess for noniterative adaptive focusing algorithm based on existing phase aberration data

The effects that each of the initial correction estimate approaches have on focal spot relative intensity are shown in Fig. 9(a). The changes in the number of ZP modes necessary to achieve 90% of nonaberrated intensity after applying the different initial estimates are shown in Fig. 9(b). Using an initial correction estimate calculated with Method 1, which takes the average of the four subjects as the initial correction for the fifth subject, increases intensity at the focal spot compared to no initial correction only for subjects 1, 2, and 3, and reduces intensity for the other two subjects. For subjects 2–5, applying Method 1 to calculate the initial estimate increases the number of ZP modes necessary to achieve 90% of nonaberrated intensity. Using an initial estimate calculated with Method 2, which computed the initial estimate as the average of the subjects from the same subgroup only, increases the initial intensity for all five subjects. However, using this initial correction increases the number of ZP modes necessary to achieve 90% of nonaberatted intensity for all five subjects, with more than 100 additional ZP modes needed for subjects 4 and 5.

V. DISCUSSION

This work serves as an initial exploration into the use of Zernike polynomials to accelerate the ultrasound phase

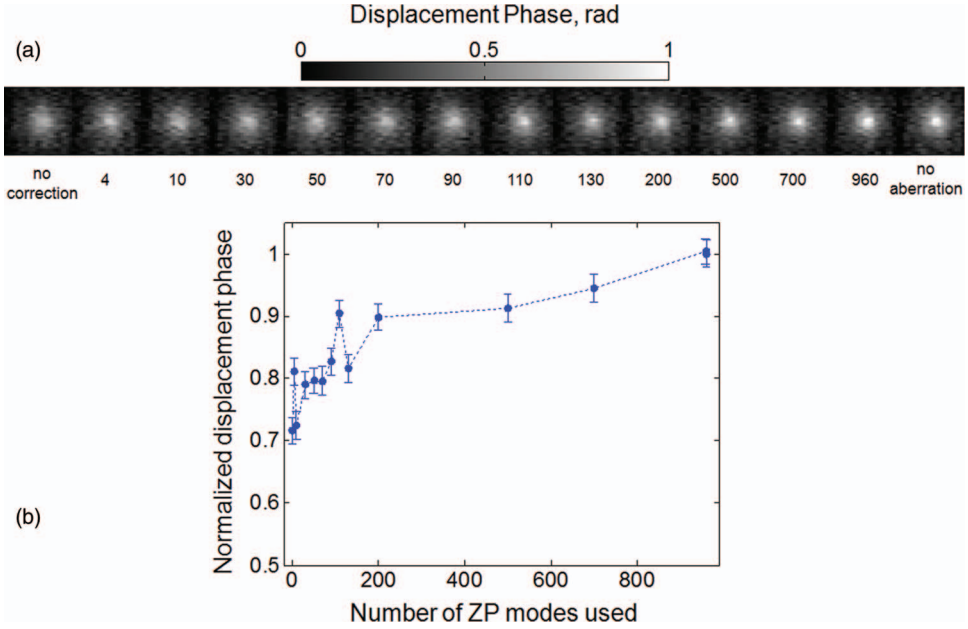

FIG. 8. Experimental validation of aberration correction for subject 1. (a) Displacement phase maps measured at the focal plane using MR-ARFI for aberration correction calculated for increasing number of ZP modes used. (b) Normalized mean displacement phase measured at the acoustic focus over a region of interest of 3 by 2 pixels. Results are displayed as mean ± standard deviation of background displacement phase noise.

aberrations correction process, potentially without the use of ionizing radiation. Applying a Zernike-based correction algorithm to compensate for the phase aberrations of five patients showed that a majority of the correction was achieved by fitting aberrations with low modes of ZP, using 170 or fewer modes to achieve 90% of the nonaberrated intensity. With four intensity measurements required to estimate each p_i^Z, in the context of using displacement phase images to drive this focusing algorithm, only $4 \times 170 = 680$ MR-ARFI acquisitions might achieve sufficient focusing. This offers substantial time savings compared to the $4 \times 960 = 3840$ measurements that would be necessary to achieve complete correction. As Zernike-based adaptive focusing requires continuous amplitude modulation, it is thus best suited for transducers with that capability.

The improvement in acoustic intensity at the focal spot after application of Zernike-based corrections was demonstrated in simulations using aberration data from five subjects. The intensity at the focal spot obtained during Zernike-encoded ultrasound emission was the highest when encoding with the lower modes, and then it decreased with the increasing Zernike polynomial mode. Therefore, prior to performing the MR-ARFI measurements of all the Zernike-encoded emissions, it would be important to select the imaging parameters that maximize the SNR of the displacement phase image of a high mode Zernike-encoded emission.

The effect of the Zernike-based phase correction on the focal acoustic intensity was experimentally visualized by measuring the displacement phase at the focal spot using MR-ARFI. The SNR of the displacement phase at the focal spot measured here was comparable to the displacement phase SNR of 20.2 measured in *ex vivo* brain tissue in the absence of the skull using an alternative transcranial focused ultrasound system.[19] In the presence of a skull, the SNR of displacement phase images will be lower which may lead to inaccurate estimates of the pressure at the focal point p_i^Z and ineffective phase correction, as was shown by Marsac *et al.* Therefore, increasing the beam intensity at the focal spot prior to making displacement phase measurements for an adaptive focusing algorithm would improve the SNR of MR-ARFI images and allow for better estimation of correction values. That is the reason why we explored the use of phase aberration data from previous patients to provide an initial correction estimate for a new subject, which could in one step improve the transducer focusing and increase the intensity at the focal spot. Using the phase aberration data from five subjects, we found that phase aberrations amongst some subjects are much more correlated than with other subjects. Here, the subjects fell into two subgroups: 1, 2, 3—into one group, and 4 and 5—into another. Making an initial correction estimate based on the data from other subjects within their subgroup led to an improved initial intensity in each of the five cases. When using less than a full set of Zernike polynomials, the initial guess serves as an estimate of the unmeasured higher order coefficients, and can therefore change how many measurements are necessary to achieve a particular level of full intensity. In this study, to achieve 90% of the full intensity, for some of the subjects, fewer ZP modes were needed thanks to the initial guess. And for other subjects, there was a need for a greater number of ZP modes. In practice, this kind of initial estimate would result in more accurate estimation of ZP correction coefficients, but require a greater number of measurements to achieve satisfactory correction. This is a tradeoff, one would consider on a case by case basis, depending on the initial SNR of displacement phase image for a particular subject's skull aberration.

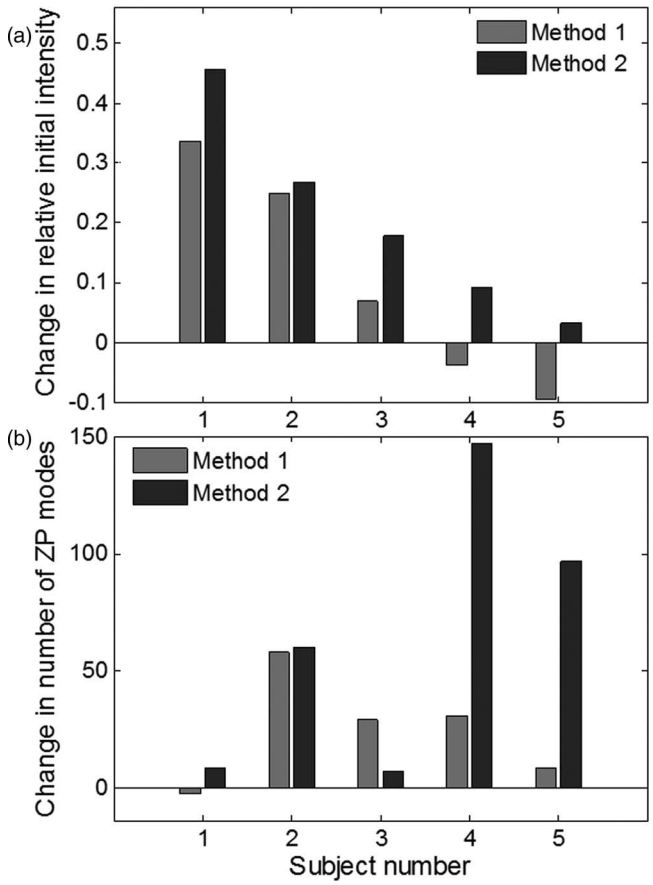

FIG. 9. Effects of the initial estimate for calculating aberration correction using two methods. In Method 1, the initial estimate of phase correction for each subject was constructed as the average of the other four subjects' aberrations. In Method 2, the subjects were divided into two subgroups: subjects 1,2,3 and subjects 4,5. In Method 2, the initial estimate was the average of the phase corrections of the remaining subjects in the subgroup. (a) Change in the initial intensity at the focal spot, as the difference in acoustic intensity at the focus with the initial guess of phase correction and without initial guess relative to the aberrated case. (b) Change in the number of ZP modes necessary to achieve 90% of intensity of the nonaberrated case relative to the default method that uses no initial guess.

Further studies of initial phase correction estimates' effectiveness would help to transition this work into a clinical setting. First, a larger population of skull measurements should be analyzed. Two distinct groups were observed when analyzing correlation between the five subjects studied here. However, once a larger population of skull measurements is analyzed, it may be determined that all skulls are unique and no similarity patterns arise. Or it may be found that a small number of representative skulls can give appropriate initial estimates for the large majority of subjects. Alternatively, it may be found that certain low-mode Zernike-based corrections are largely consistent across the population, which would allow for a common low-mode correction to be used as an initial estimate for each new subject. It would also be of interest to explore MR images of a skull as a way to associate a new patient with an appropriate initial estimate of aberrations based on a subgroup of similar skulls. In future work, the effects of noise and blurring (due to shear waves and other effects) in the displacement phase measurements on the performance of this adaptive focusing algorithm need to be assessed. Finally, the use of spherical harmonics for characterizing aberrations and corrections should also be explored. It may be the case that spherical harmonics offer even greater correction efficiency, either in place of or in combination with Zernike polynomials.

In this work, the application of Zernike polynomials to phase aberration correction was shown to be beneficial for adaptive focusing applications of transcranial ultrasound. Simulation and experimental results showed that skull-based phase aberrations can be well approximated by a number of ZPs representing only a fraction ($<20\%$) of the number of elements in the hemispherical ultrasound transducer, which would allow for more than a $5\times$ speedup in aberration correction as compared to full sampling approaches proposed before. The concentration of relative contribution to phase aberration correction at lower mode ZPs and the improvement of intensity at the focal spot after correction with an initial estimate may make the Zernike-based approach introduced here more robust to MR-ARFI measurement noise. These improvements can potentially greatly increase the viability of MR-ARFI-based adaptive focusing for a clinical transcranial MRgFUS therapy.

ACKNOWLEDGMENTS

The authors thank InSightec Ltd. for making a system available for model validation, and Rachel R. Bitton, Adam Wang, and John Pauly for valuable discussions about ultrasound focusing and Zernike encoding. National Institutes of Health (NIH) Grant Nos. R21 EB011559 and PO1 CA159992.

[a]Author to whom correspondence should be addressed. Electronic mail: klena@stanford.edu

[1]C. M. C. Tempany *et al.*, "MR imaging-guided focused ultrasound surgery of uterine leiomyomas: A feasibility study," Radiology **226**(3), 897–905 (2003).
[2]K. Hynynen *et al.*, "MR imaging-guided focused ultrasound surgery of fibroadenomas in the breast: A feasibility study," Radiology **219**(1), 176–185 (2001).
[3]H. Furusawa *et al.*, "The evolving non-surgical ablation of breast cancer: MR Guided focused ultrasound (MRgFUS)," Breast Cancer **14**(1), 55–58 (2007).
[4]D. Gianfelice *et al.*, "MR imaging-guided focused US ablation of breast cancer: Histopathologic assessment of effectiveness-initial experience," Radiology **227**(3), 849–855 (2003).
[5]R. O. Illing *et al.*, "The safety and feasibility of extracorporeal high-intensity focused ultrasound (HIFU) for the treatment of liver and kidney tumours in a Western population," Br. J. Cancer **93**(8), 890–895 (2005).
[6]E. Martin *et al.*, "High-intensity focused ultrasound for noninvasive functional neurosurgery," Ann. Neurol. **66**(6), 858–861 (2009).
[7]N. McDannold *et al.*, "Transcranial magnetic resonance imaging-guided focused ultrasound surgery of brain tumors: Initial findings in 3 patients," Neurosurgery **66**(2), 323–332 (2010).
[8]G. T. Clement *et al.*, "A hemisphere array for non-invasive ultrasound brain therapy and surgery," Phys. Med. Biol. **45**, 3707–3719 (2000).
[9]G. T. Clement, J. White, and K. Hynynen, "Investigation of a large-area phased array for focused ultrasound surgery through the skull," Phys. Med. Biol. **45**, 1071–1083 (2000).
[10]G. T. Clement *et al.*, "A magnetic resonance imaging-compatible, large-scale array for trans-skull ultrasound surgery and therapy," J. Ultrasound Med. **24**(8), 1117–1125 (2005).

[11]J. Sun and K. Hynynen, "Focusing of therapeutic ultrasound through a human skull: A numerical study," J. Acoust. Soc. Am. **104**(3), 1705–1715 (1998).
[12]K. Hynynen and J. Sun, "Trans-skull ultrasound therapy: The feasibility of using image-derived skull thickness information to correct the phase distortion," IEEE Trans. Ultrason. Ferroelectr. Freq. Control **46**(3), 752–755 (1999).
[13]M. Pernot *et al.*, "Experimental validation of 3D finite differences simulations of ultrasonic wave propagation through the skull," paper presented at the 2001 IEEE International Ultrasonics Symposium (unpublished).
[14]G. T. Clement and K. Hynynen, "A non-invasive method for focusing ultrasound through the human skull," Phys. Med. Biol. **47**(8), 1219–1236 (2002).
[15]G. T. Clement and K. Hynynen, "Correlation of ultrasound phase with physical skull properties," Ultrasound Med. Biol. **28**(5), 617–624 (2002).
[16]J.-F. Aubry *et al.*, "Experimental demonstration of noninvasive transskull adaptive focusing based on prior computed tomography scans," J. Acoust. Soc. Am. **113**(1), 84–93 (2003).
[17]B. Larrat *et al.*, "MR-guided adaptive focusing of ultrasound," IEEE Trans. Ultrason. Ferroelectr. Freq. Control **57**(8), 1734–1747 (2010).
[18]Y. Hertzberg *et al.*, "Ultrasound focusing using magnetic resonance acoustic radiation force imaging: Application to ultrasound transcranial therapy," Med. Phys. **37**(6), 2934–2942 (2010).
[19]L. Marsac *et al.*, "MR-guided adaptive focusing of therapeutic ultrasound beams in the human head," Med. Phys. **39**(2), 1141–1149 (2012).
[20]A. P. Sarvazyan *et al.*, "Shear wave elasticity imaging: A new ultrasonic technology of medical diagnostics," Ultrasound Med. Biol. **24**(9), 1419–1435 (1998).
[21]N. McDannold and S. E. Maier, "Magnetic resonance acoustic radiation force imaging," Med. Phys. **35**(8), 3748–3758 (2008).
[22]M. Radicke *et al.*, *Hyperfine Interactions* (Springer, Netherlands, 2008), Vol. 181, p. 21.
[23]F. Zernike, "Beugungstheorie des Schneidenverfahrens und seiner verbesserten Form, der Phasenkontrastmethode," Physica **1**, 689–704 (1934).
[24]M. J. Booth, M. A. A. Neil, and T. Wilson, "Aberration correction for confocal imaging in refractive-index-mismatched media," J. Microsc. **192**(2), 90–98 (1998).
[25]D. L. Fried, "Statistics of a geometric representation of wavefront distortion," J. Opt. Soc. Am. **55**(11), 1427–1435 (1965).
[26]R. J. Noll, "Zernike polynomials and atmospheric turbulence," J. Opt. Soc. Am. **66**(3), 207–211 (1976).
[27]H. C. Howland and B. Howland, "A subjective method for the measurement of monochromatic aberrations of the eye," J. Opt. Soc. Am. **67**(11), 1508–1518 (1977).
[28]A. Bhatia and E. Wolf, "The Zernike circle polynomials occurring in diffraction theory," Proc. Phys. Soc. B **65**, 909–910 (1952).
[29]D. Malacara, *Optical Shop Testing*, 3rd ed. (Wiley-Interscience John Wiley & Sons, Inc., Hoboken, 2007).
[30]P. Fricker, MATLAB Central File Exchange, 2005.
[31]M. Pap, "Discrete orthogonality of Zernike functions," Math. Pannonica **16**(1), 137–144 (2005).
[32]J. Allen, Orthogonality and convergence of discrete Zernike polynomials, Ph.D. thesis, University of New Mexico, 2010.
[33]E. A. Kaye and K. Butts Pauly, "Adapting MRI acoustic radiation force imaging for in vivo human brain focused ultrasound applications," Magn. Reson. Med. (Early View).
[34]J. Rayleigh, *The Theory of Sound* (Dover Publications, New York, 1945).
[35]E. A. Kaye, J. Chen, and K. B. Pauly, "Rapid MR-ARFI method for focal spot localization during focused ultrasound therapy," Magn. Reson. Med. **65**(3), 738–743 (2011).